A new K-band (18 - 26 GHz) 7-horn multi-feed receiver: Calibration campaign at Medicina 32 m dish

R.Verma, G.Maccaferri, A.Orfei
I.Prandoni, L.Gregorini

IRA 430/09

Contents

List of Tables

List of Figures

Chapter 1

1.1 Goals

This report describes the results of the calibration campaign carried out in K-band (18 - 26 GHz) with the new 7-horn multi-feed receiver mounted on Medicina 32 m dish. The multi-feed is designed to perform high sensitivity continuum observations, spectroscopy and polarimetry and is optimized for the upcoming new 64m Sardinia radio Telescope. Since the SRT is under construction, the multi-feed has been mounted on Medicina 32m dish to test and calibrate the instrument.

The Medicina telescope is equipped with many receivers: ones working at 1.4 GHz, 8 GHz and 22 GHz are mounted on the primary focus of the telescope while, the one working at 5 GHz and the K-band multi-feed are mounted on the cassegrain focus of the dish. The main target of this work is the description of the procedure to calibrate the 7-horn multi-feed receiver. It is essential (and done as a routinely work) to check the pointing of any receiver and to retrieve a pointing model for it once it is mounted on the telescope. It is also required to provide to telescope users antenna parameters and gain curve *as a priori*.

This compendium has to be referred as a repository for all the information related to the pointing and gain calibration of the K-band multi-feed receiver.

1.2 Methods

In order to calibrate the multi-feed receiver we have to go through two steps:

Pointing and focus

The first step of the calibration procedure is to check the pointing and focus of the receiver. This is known as the pointing calibration in antenna system terminology.

In order to check the telescope pointing one should first check the optics of the antenna. The mirrors[1] and feed should be in alignment.

Antenna measurements

After the pointing calibration we can determine the antenna characteristic parameters: system temperature, spillover temperature, antenna temperature and antenna gain, by observing an astronomical source. This allows us to provide the antenna performance to the users of the multi-feed.

1.3 Antenna terminology

We will use the following terminology in this document:

- 'AX_0', 'AY_0', '$AZ1_0$', '$AZ2_0$', and '$AZ3_0$' refer to 'the position of X, Y, Z1, Z2 and Z3 actuators in mm at an elevation of 45° where the subreflector is aligned with the primary reflector'
- 'AX', 'AY', 'AZ1', 'AZ2', and 'AZ3' refer to 'the amount of displacement with respect to the primary reflector to get the final position parameters of the subreflector x, y , z , θ_x and θ_y'
- 'Ag' refers to 'geometric area'
- 'd_{sky}' refers to 'sky distance between the horns of multi-feed'
- 'd' refers to 'physical distance between the horns of multi-feed'
- 'D' refers to 'diameter of the dish'
- 'El' refers to 'elevation'
- 'f' refers to 'focal length of cassegrain focus'
- 'G' refers to 'antenna gain'
- 'HPBW' refers to 'half power beam width'
- 'k_B refers to 'Boltzmann constant'
- 'LCP' refers to 'left circular polarization'

[1] primary mirror, secondary mirror

- 'm'= 0.5 (non polarized radiation)
- 'η_A' refers to 'antenna efficiency'
- 'η_{bloc}' refers to 'blocking efficiency'(consists of two terms: first due to secondary reflector and second due to struts)
- '$\eta_{blocSec}$' refers to 'blocking efficiency due to secondary reflector'
- '$\eta_{blocSrut}$' refers to 'blocking efficiency due to Struts'
- 'η_{diffr}' refers to 'diffraction loss efficiency'
- 'η_{floss}' refers to 'feed loss efficiency'
- 'η_{ph}' refers to 'phase efficiency'
- 'η_{sloss}' refers to 'surface loss efficiency'
- 'η_{spill}' refers to 'spillover efficiency'
- 'η_{surf}' refers to 'surface efficiency'
- 'η_{taper}' refers to 'taper efficiency'
- 'η_{vswr}' refers to 'feed return loss efficiency'
- 'η_x' refers to 'cross polarization efficiency'
- 'P' refers to 'total power per unit bandwidth at the terminal of the antenna'
- 'RCP' refers to 'right circular polarization'
- 'σ' refers to the 'total rms error on the surface accuracy due to primary mirror panels, secondary mirror panels, gravity deformation and panel alignment error'
- 'σ_{Align} ' refers to the 'rms error in the alignment of mirror panels'
- '$\sigma_{Gravity}$ ' refers to the 'rms error on the surface accuracy due to gravity deformation'
- 'σ_P ' refers to the 'rms error on the surface accuracy due to primary mirror panels'
- 'σ_{Sec} ' refers to the 'rms error on the surface accuracy due to secondary mirror panels'
- 'T', refers to 'the taper of the receiver'

- 'T_a' refers to 'antenna temperature '
- 'T_{atm}' refers to 'Mean value of atmospheric temperature'
- 'T_{CMB}' refers to 'background sky brightness'(CMB $\approx$ 3K)
- 'T_{cover}'refers to 'temperature of the cover placed on the multi-feed receiver.It contributes approximately 5 K to the system temperature in K-band'
- 'τ' refers to atmospheric 'opacity'.
- 'T_{sky}' refers to 'sky contribution to the system temperature'
- 'T_{spill}' refers to 'spillover temperature'
- 'T_{sys}' refers to 'system temperature of the antenna'
- '$T_{receiver}$' refers to 'noise temperature of the receiver'
- 'θ_x'and 'θ_y' refer to the angle of tilt about X-axis and Y-axis respectively.
- 'λ' refers to 'observing wavelength'
- 'X_{air}' refers to 'airmass'
- 'x' 'y' represent the azimuth and elevation axis respectively
- 'z' refers to 'the focus axis of the telescope'

Chapter 2

New 7-horn multi-feed receiver at Medicina

In this chapter we present a brief description of the 7-horn multi-feed receiver. We also present the definitions of the antenna parameters and their estimated value obtained with laboratory measurements and simulations.

2.1 K-band multi-feed receiver

The new K-band multi-feed receiver is a seven horn focal plane array arranged in a hexagon with a central feed. It consists of seven corrugated feeds working in (18-26 GHz) K-band providing fourteen output channels (LCP and RCP for each feed) with an instantaneous bandwidth up to 2 GHz. The K-band multi-feed receiver is shown in Figures 2.1 & 2.2 . Its characteristic parameters are listed in Table 2.1

Table 2.1: 22 GHz multi-feed receiver characteristics

Inner Diameter of the feeds	68.8 mm
Outer Diameter of the feeds	98.0 mm
Distance between two adjacent feeds	100.0 mm
Output channels	14 [a] (7 LCP + 7 RCP with 2 GHz-wide IF bands)

[a]presently channels 6 RCP & 4 LCP are not working

Figure 2.1: Top view of multi-feed receiver

Figure 2.2: Multi-feed receiver with feeds numbered

2.2 Antenna parameters

Before presenting the laboratory measurements and the simulations of the multi-feed parameters, it is useful to define the antenna parameters relevant for this work.

2.2.1 System temperature

The system temperature of an antenna can be defined as a measure of total noise contribution in the system when observing a blank sky. Since the noise coming from sub systems forming the telescope is uncorrelated, the different noise contributions add up linearly. We can represent the system temperature as below:

$$T_{sys} = T_{receiver} + T_{cover} + T_{sky} + T_{spill} + T_{CMB} \tag{2.1}$$

and T_{sky} can be represented as

$$T_{sky} = T_{atm} * [1 - e^{-(\tau X_{air})}] \tag{2.2}$$

$$X_{air} = \frac{1}{\cos(90 - El)} \tag{2.3}$$

2.2.2 Spillover temperature

The feed is supposed to collect the radiation focused by the reflector but often it also picks up stray radiation beyond the edge of reflector. This contribution is known as spillover temperature. Spillover temperature in a dual (primary and secondary) reflector antenna has two components described below and shown in Figure 2.3:
(i) the feed spillover beyond the rim of the subreflector known as forward spillover;
(ii) the scattered radiation past the rim of the main reflector known as rear spillover.

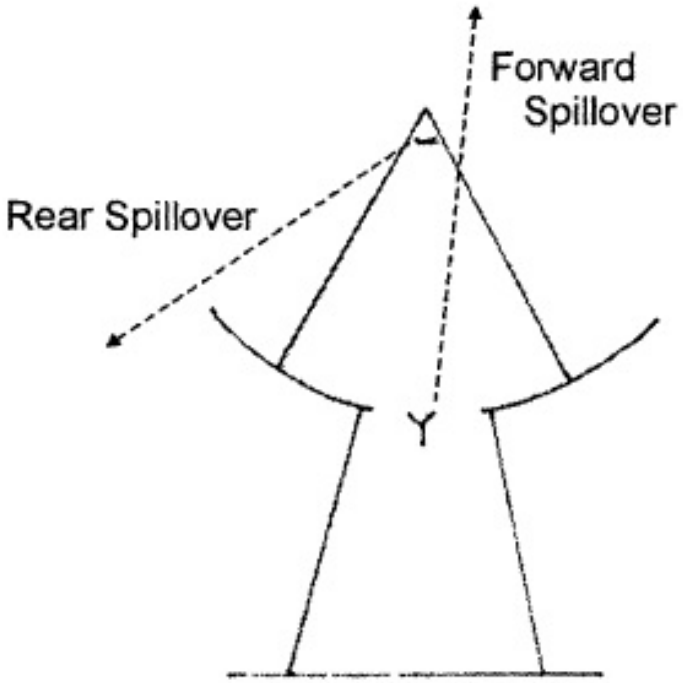

Figure 2.3: Pictorial view of the spillover temperature of the antenna

2.2.3 Antenna temperature

The Antenna temperature T_a is a measure of the signal strength in radio astronomy. It is defined as the temperature of a black-body enclosure which, if completely surrounding a radio telescope, would produce the same signal power as the source under observation. The mathematical expression can be given by:

$$P = k_B T_a \tag{2.4}$$

2.2.4 Antenna Gain

The antenna gain is defined as :

$$G = 10^{-26} \frac{m \eta_A A_g}{k_B} [\frac{K}{Jy}] \tag{2.5}$$

For the Medicina antenna, the constant

$$10^{-26} \frac{m A_g}{k_B} \approx 0.292 \tag{2.6}$$

The antenna efficiency considering all the degradation factors can be defined as follows:

$$\eta_A = \eta_{bloc} * \eta_x * \eta_{ph} * \eta_{spill} * \eta_{diffr} * \eta_{taper} * \eta_{surf} * \eta_{floss} * \eta_{vswr} * \eta_{sloss} \tag{2.7}$$

and
η_{surf} can be given by,

$$\eta_{surf} = e^{-(4\pi \frac{\sigma}{\lambda})^2} \tag{2.8}$$

where

$$\sigma \approx \sqrt{\sigma_P^2 + \sigma_{Sec}^2 + \sigma_{Gravity}^2 + \sigma_{Align}^2} \tag{2.9}$$

and $\sigma_{Gravity}$ varies with elevation.

2.3 Laboratory measurements & simulations

In this section we present the multi-feed receiver parameters (system temperature, antenna gain, HPBW of the antenna, sky distance between adjacent beams) as obtained from laboratory measurements and simulations.

2.3.1 System temperature

The receiver temperature of the multi-feed receiver has been measured in the laboratory using hot and cold load[1]. By assuming for the other factors contributing to the system temperature (see eq. 2.1):
$T_{cover} = 5$ K, **Measured** (The receiver is covered to protect it from the outside ambient).
$T_{spill} = 5 - 7$ K, **Estimated**
$T_{atm} = 278$ K, **Estimated**
$\tau = 0.1$ **Estimated** (Average opacity during the year)

We obtained $T_{sys} \approx 75$ K for the central horn at an El of 45°

2.3.2 Antenna gain

The antenna gain for the central and lateral feeds was estimated through simulations with the following assumptions[1] (see eq. 2.7):

Table 2.2: Antenna Efficiency parameters of multi-feed receiver at 22 GHz

Efficiency	**In axis**[a] (%)	**Off-axis**[b] (%)
η_{taper}	95.7	95.6
η_{ph}	99.3	99.3
η_{spill}[c]	70.4	70.3
$\eta_{blocSec}$	97.3	97.2
$\eta_{blocSrut}$	94.0	94.0
$\eta_x * \eta_{diffr} * \eta_{sloss}$	98.0	98.0
η_{floss}	92.0	92.0
η_{vsrw}	99.0	99.0
η_{surf}	See below	See below

[a] Central feed
[b] lateral feeds
[c] It consist of two contributions: Spillover efficiency of primary reflector, and Spillover efficiency of secondary reflector

The surface efficiency is described by a Gaussian function (see eq.2.8), therefore a small error in estimating this factor can severely affect the overall efficiency of the antenna and can degrade the antenna gain.
The components contributing to the rms error σ for the Medicina dish are given below :

[1] a.orfei@ira.inaf.it, Private Communication

$\sigma_P = 0.40$ mm
$\sigma_{Sec} = 0.35$ mm
$\sigma_{Align} = 0.2$ mm
$\sigma_{Gravity} = \sqrt{\sigma_{90}^2 + \sigma_{60}^2 + \sigma_{45}^2 + \sigma_{30}^2 + \sigma_{20}^2} = 0.70$ mm

where the factors contributing to $\sigma_{Gravity}$ are listed in the following table:

Table 2.3: Rms error due to gravity deformation as a function of elevation

Elevation (degree)	**rms error due to gravity deformation**[a] **(mm)**
90	0.58
60	0.19
45[b]	0.00
30	0.25
20	0.40

[a]For our calculation we have considered a 20% increase on each measurement to keep into consideration the degradation due to the aging of the telescope structure

[b]at this elevation panel alignment is done

With these assumptions the antenna gain is 0.105[2] K/Jy for both central and lateral feeds.

2.3.3 HPBW of the each horn

The HPBW of the feed is calculated as :

$$HPBW = (1.02 - 0.00135 * T) * \lambda / D \tag{2.10}$$

T = -5.3 dB, for the multi-feed at 22 GHz.
λ = 1.36 cm (corresponding to 22 GHz).

The calculated HPBW of each horn is 92" at 22 GHz.

[2]This value corresponds to an elevation of 45°

2.3.4 Sky distance between two adjacent horns

The sky distance between two adjacent horns is given by:

$$d_{sky} = d/f = 212" \tag{2.11}$$

where for the multi-feed receiver:
d = 100 mm
f = 97.36 m

2.3.5 Summary of lab measurements and simulations

The antenna parameters obtained from laboratory measurements and expected by simulations describing the receiver performance at Medicina, are listed in the Table 2.4

Table 2.4: Antenna performance parameters

System temperature (El = 45°, $\tau = 0.1$)	75 K (central horn)
Antenna gain (central & lateral horns)	0.105 K/Jy ($\sigma = 0.70$)
HPBW	92"
Sky distance between the horns	212"

Chapter 3

Pointing & gain calibration: Test measurements

In this chapter we present the test measurements obtained by observing an astronomical source in order to retrieve a pointing model for the multi-feed receiver and to better characterize the receiver performance at Medicina.

3.1 Pointing calibration

There are many parameters, for example surface accuracy, thermal deformation, gravity, pointing errors and focusing, that can limit the high frequency performance of the antenna. Pointing accuracy becomes important at high frequency, since the maximum errors allowed in the sky coordinates (α, δ) should always satisfy the condition $[(\sigma_\alpha \cos\delta)^2 + (\sigma_\delta)^2]^{\frac{1}{2}} \leq \frac{HPBW}{10}$; and higher the frequency smaller the half power bandwidth (HPBW) of the antenna beam.

Typically a telescope beam pattern is considered to be Gaussian. Therefore a significant relative offset between the telescope pointing direction and the actual source position can result in a significant reduction of the telescope gain, as shown in Figure, 3.1 (a). This can severely affect the signal to noise ratio (SNR) and the calibration of the observation . In addition, in presence of poor focus of the telescope the source gets diffused and is not concentrated at the center of the antenna beam where the telescope gain is maximum (Figure 3.1 (b)). This can also degrade the object's SNR.

Figure 3.1: Effect of Pointing error & Poor focus of the telescope

3.1.1 Optical alignment

After the multi-feed receiver was mounted on Medicina 32 m dish, we checked the optical alignment to determine the telescope's pointing accuracy for the multi-feed receiver. In order to check the optical alignment we performed cross-scans across the point like source W3OH[1] at 22 GHz using the VLBI acquisition system with the mechanically determined optical alignment[2]. From our first measurements we found that the antenna beam is not symmetric in azimuth and elevation axes. This is shown in Figure 3.2 where the green line shows the elevation scan of W3OH while the red one shows the azimuth scan at an elevation of 33°. The antenna beam is asymmetric in azimuth and elevation axes and there are sidelobes present in both the axes. This beam asymmetry in azimuth and elevation axes implies that the telescope optics (primary mirror, secondary mirror and feed) is not aligned properly.

3.1.2 Strategy adopted to get the optical alignment for multi-feed receiver

The multi-feed is mounted on the secondary focus. Therefore one can try to better align the optics by moving the subreflector. The subreflector is equipped with five actuators providing five degrees of freedom for the movement: three degrees for translation - east-west (X-axis), north-south (Y-axis) and Z-axis and two degrees of freedom for tilting.
Figure 3.3 shows the subreflector geometry. The movements in X & Y directions are done using X & Y actuators while tilting and focusing is done by moving Z1, Z2, and Z3 actuators situated at the

[1] W3OH is a circumpolar source which is very bright at 22 GHz

[2]The mechanically determined optical alignment refers to the alignment done using an optical collimator when mounting the receiver on the telescope

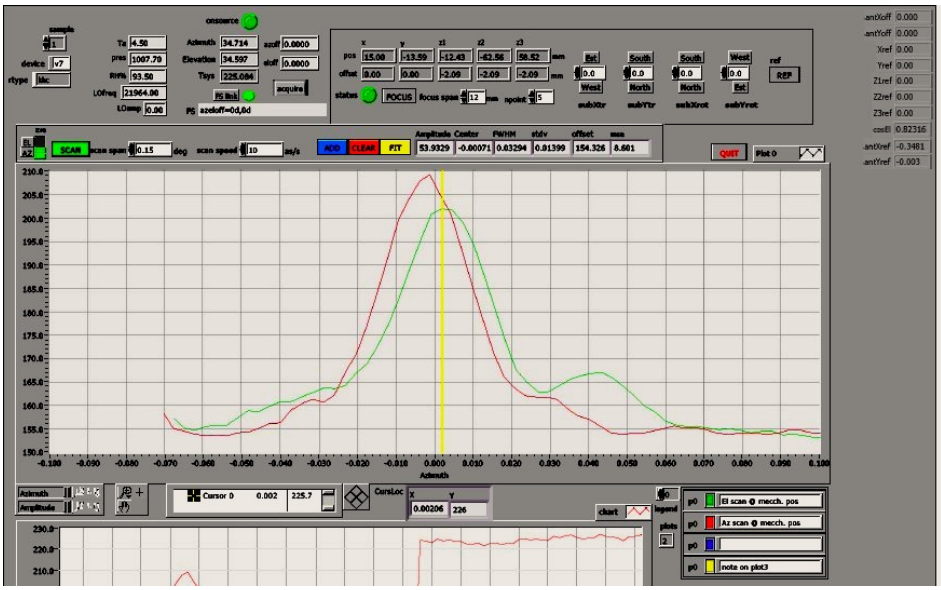

Figure 3.2: Cross scans on source W3OH. Green line shows the elevation scan and red line shows the azimuth scan (at an elevation of 33°)with the mechanically determined optical alignment. The X-axis represents the offset (in degrees) between the telescope pointing direction and the source position, Y-axis denotes the temperature of the source. The antenna beam is asymmetric in elevation and azimuth axes having an offset relative to each other. A significant sidelobe is also present in the elevation axis

vertices of an isosceles triangle. A zoomed view of the Z-axis actuator positions is shown in Figure 3.4 where Z1, Z2, Z3 are the positions of the actuators ; O is the centre of the isosceles triangle. L and r are the base and height of the triangle respectively. h is the height of the centre of triangle. The equation of motion for the subreflector can be given by

$$x(mm) = AX - AX_0 \tag{3.1a}$$

$$y(mm) = 0.9903 * (AY - AY_0) \tag{3.1b}$$

$$z(mm) = 0.1392 * (AY - AY_0) + 0.3333 * (AZ1 - AZ1_0) + 0.3333 * (AZ2 - AZ2_0) + 0.3333 * (AZ3 - AZ3_0) \tag{3.1c}$$

$$\theta_x(rad) = (AZ1 - AZ1_0)/1791 - (AZ2 - AZ2_0)/3582 - (AZ3 - AZ3_0)/3582 \tag{3.1d}$$

$$\theta_y(rad) = (AZ2 - AZ2_0)/2068 - (AZ3 - AZ3_0)/2068 \tag{3.1e}$$

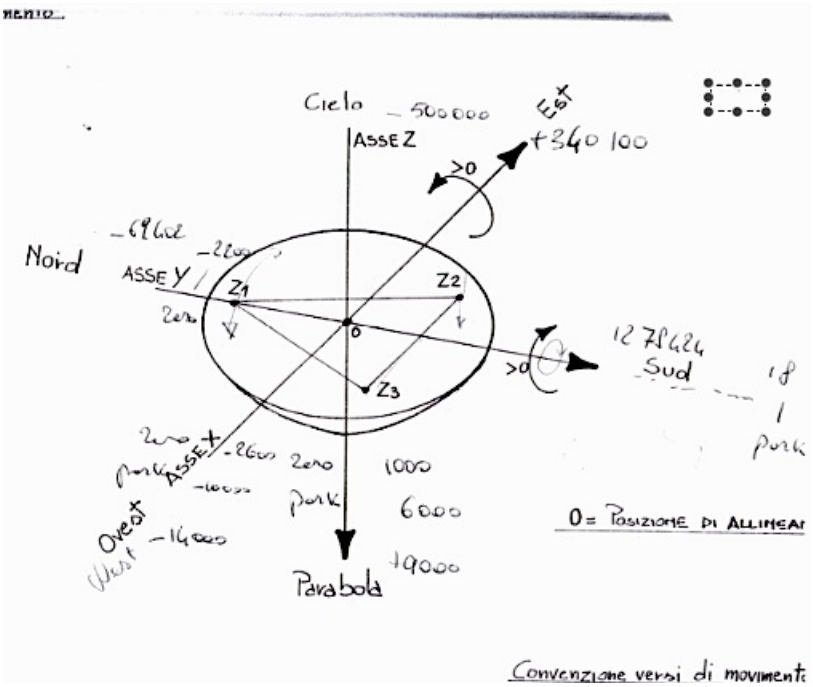

Figure 3.3: Subreflector geometry. Z1, Z2, Z3 show the position of three actuators used to tilt & focus the subreflector

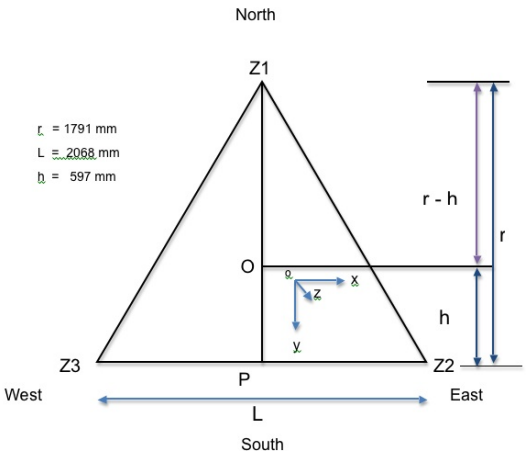

Figure 3.4: Position of the three actuators situated at the vertices of an isosceles triangle. O is the center of the triangle coinciding with the rotation axis of the subreflector

3.1.3 Results

We performed sequences of cross scans across W3OH with different subreflector positions to maximize the peak amplitude of the point source in the main lobe of the antenna beam. Measurements were done by moving the subreflector in X,Y, Z axes and tilting it about the X and Y axes to get the best alignment and focus for the multi-feed receiver. A comparison between the mechanically determined and optimized optical alignment is shown in Figure 3.5 and 3.6. Figure 3.5 shows the cross scan on W3OH with mechanically determined optical alignment. Red and green lines show the azimuth scan (at an elevation of 67°) and the elevation scan respectively. The antenna beam is asymmetric and there are sidelobes present in elevation scan.
Figure 3.6 shows the cross scan on W3OH with optimized optical alignment. Red and green lines show the azimuth scan (at an elevation of 66°) and elevation scan respectively. Figure 3.6 shows that the antenna beam is symmetric in elevation and azimuth axes with lower sidelobes. We measured a maximum increment of 30% in the peak amplitude in the main lobe of antenna beam with the optimized optical alignment.

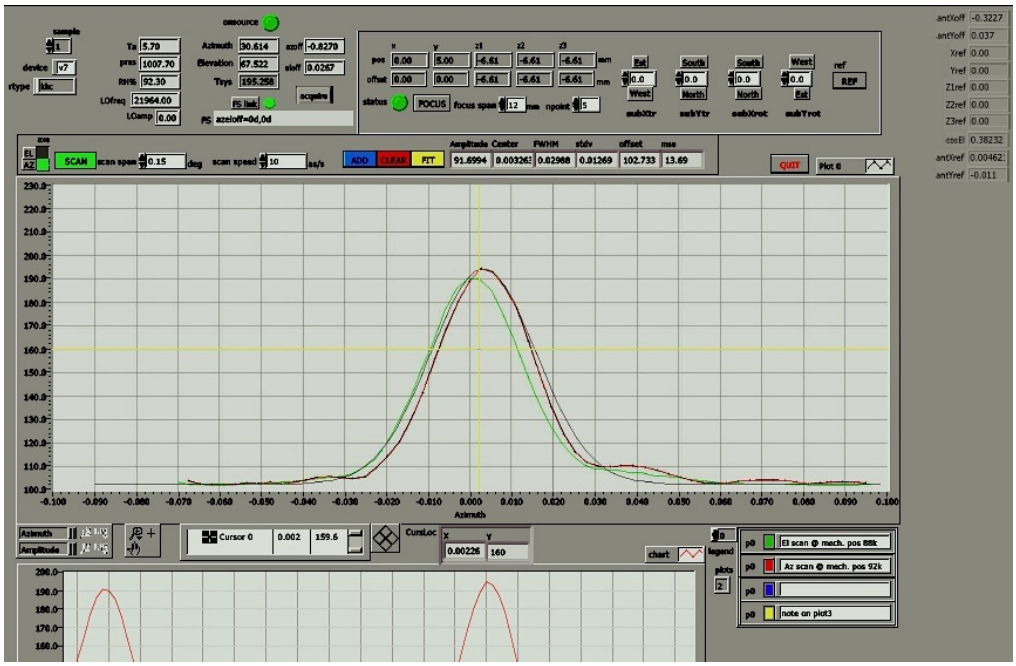

Figure 3.5: Cross scan on the source W3OH. Red line shows the azimuth scan on the source at an elevation of 67° and green line shows the elevation scan with the mechanically determined optical alignment.

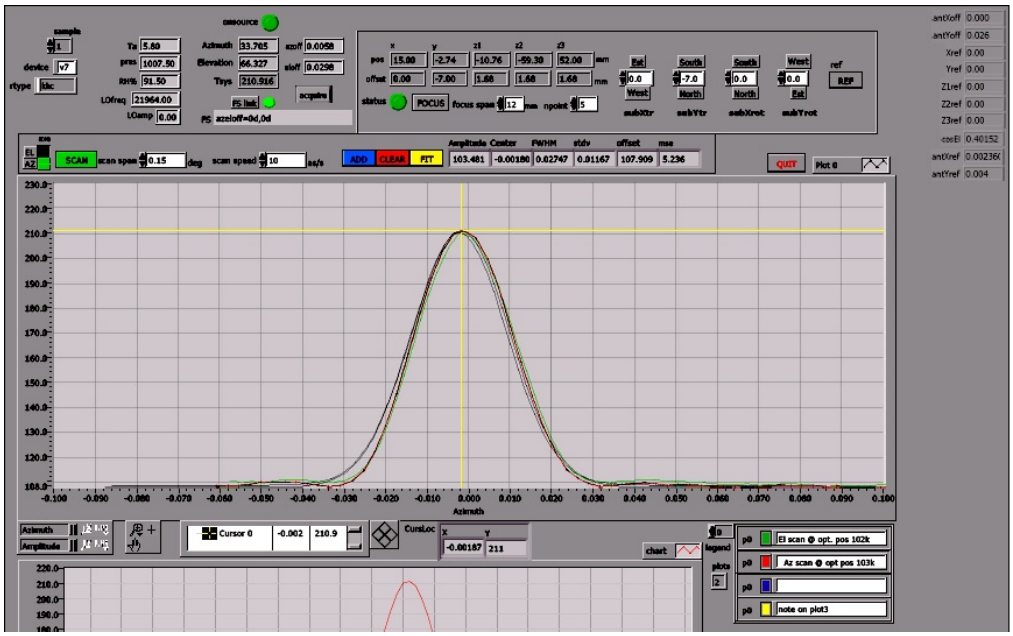

Figure 3.6: Cross scan on W3OH with optimized optical alignment. Red line shows the azimuth scan at an elevation of 66° while green line shows the elevation scan

We performed many test observations to get the optimized subreflector position parameters as a function of elevation. The subreflector position polynomials as a function of elevation for mechanically determined and optimized optical alignment are shown in Figures 3.7 and 3.8 and listed in Table 3.1. It is important to remark that to obtain the new optimized alignment we had to strongly tilt the subreflector by moving the Z3 actuator. The Z3 actuator is at the limit of its movement. We implemented the new subreflector position polynomials into the Subreflector Control Unit (SCU) model and evaluated a new pointing model observing many sources. After evaluating the new pointing model for the multi-feed receiver we implemented it in the antenna control system known as Field System.

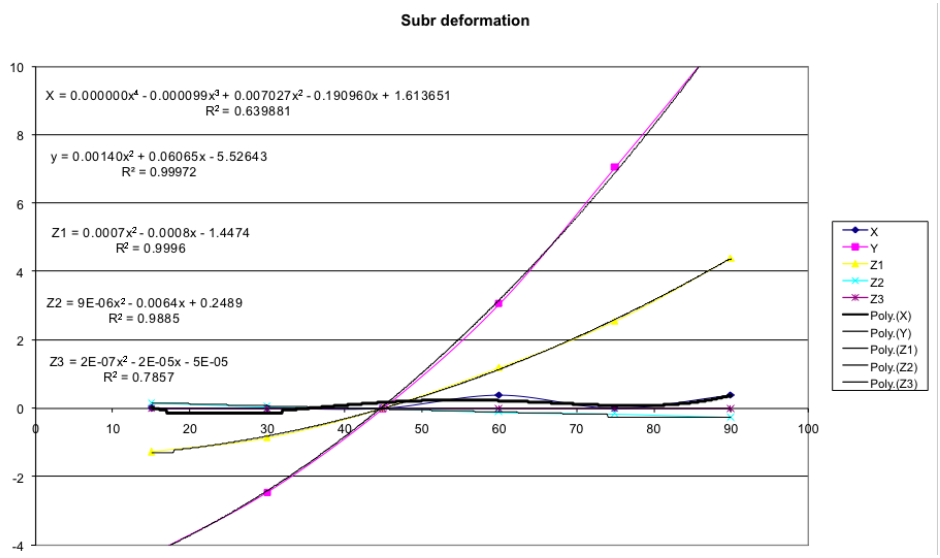

Figure 3.7: Subreflector position parameter polynomial as a function of elevation for mechanically determined optical alignment. Symbols represents the data observed to measure X,Y,Z1,Z2,Z3 parameters as a function of elevation while lines are the polynomials fitted to the data.

Table 3.1: Subreflector position polynomials for mechanical and optimized optical alignment

Subreflector position polynomial	
Mechanical optical alignment	**Optimized optical alignment**
$X^a = 0.000000x^{4b} - 0.000099x^3 + 0.007027x^2 - 0.190960x + 1.613651$	$X = 15$
$Y^c = 0.00140x^2 + 0.06065x - 5.52643$	$Y = -0.000x^2 + 0.502x - 34.73$
$Z1^d = 0.0007x^2 - 0.0008x - 1.4474$	$Z1 = -0.0026x^2 + 0.2194x - 13.809$
$Z2^e =$(9e-6)$x^2 - 0.0064x + 0.2489$	$Z2 = 0.0097x^2 - 0.976x - 37.203$
$Z3^f =$ (2e-7)$x^2 -$ (2e-5)$x -$ (5e-5)	$Z3 = -0.0035x^2 + 0.0563x + 63.439$

[a]X represents 'AX'
[b]x axis is the elevation axis.
[c]Y represents 'AY'
[d]Z1 represents 'AZ1'
[e]Z2 represents 'AZ2'
[f]Z3 represents 'AZ3'

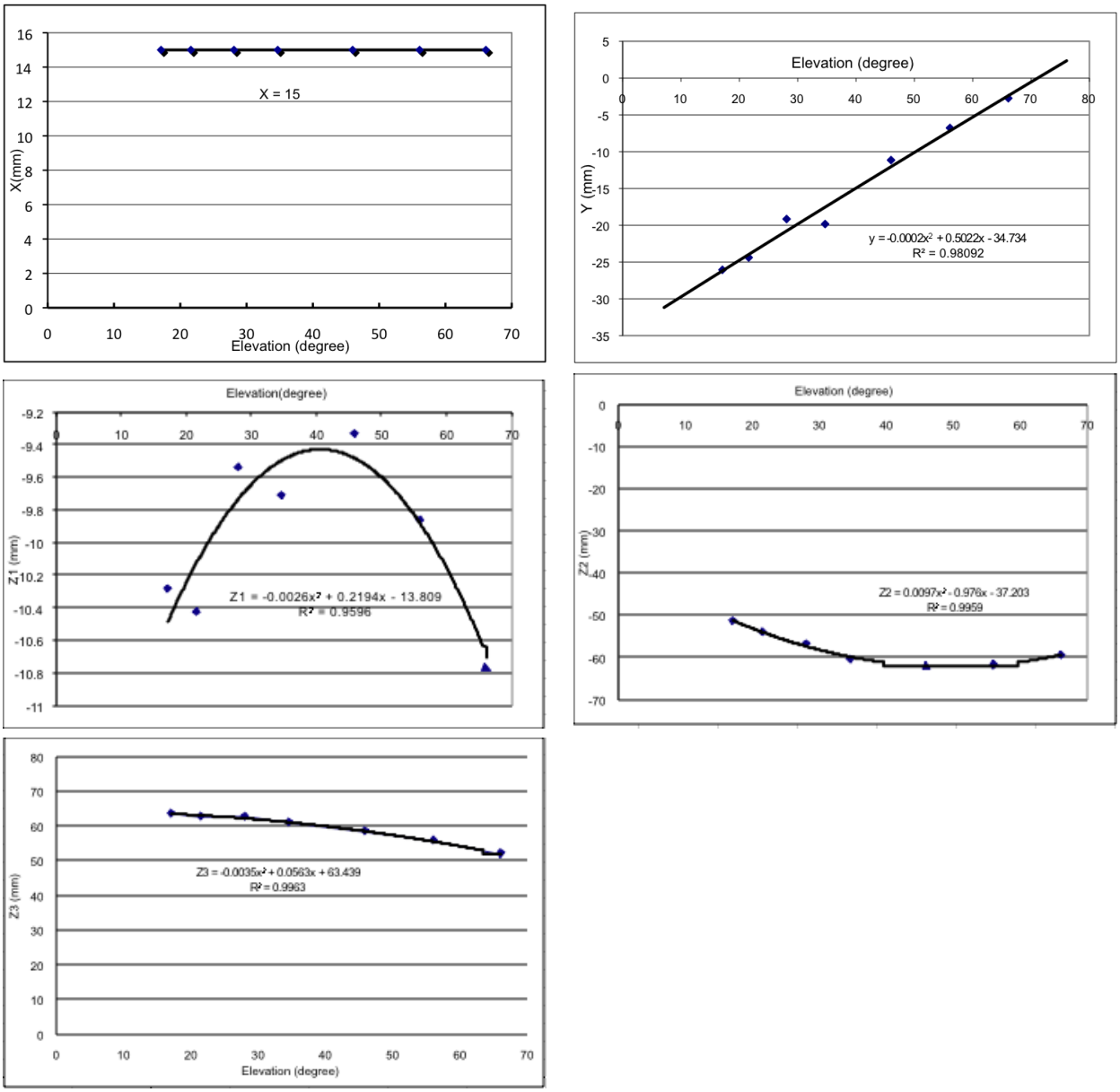

Figure 3.8: Subreflector position parameter polynomial as a function of elevation for optimized optical alignment. Diamonds are the data obtained for X, Y, Z1, Z2 and Z3 parameters vs elevation. Lines represent the polynomial fitting to the data.

3.2 Antenna measurements

In this section we present the results of test measurements performed by observing an astronomical source to measure antenna parameters like system temperature, spillover temperature and the antenna gain for the central and lateral horns[3] of multi-feed receiver.

In order to characterize astronomical observation, one should know the system temperature and the spillover temperature for the observed frequency and elevation. Therefore after implementing the new subreflector model for optimized optical alignment and the new antenna-pointing model in the Field System, we performed measurements of the system temperature and spillover temperature as a function of elevation and frequency for all the seven feeds.
Good measurements of these parameters are very important to correctly calibrate the data. Before measuring the system and spillover temperatures it is also necessary to quantify the atmospheric opacity at the observed frequency. The measurement of the atmospheric opacity quantifies the contribution of the atmosphere to the signal coming from a source.

3.2.1 System temperature and Tipping curves

The atmospheric opacity has been measured through the standard *tipping curves* which allow the noise temperature contribution of the atmosphere to be quantified. The tipping-curve data acquisition strategy involves taking a set of system temperature measurements at a series of different elevation, where elevation goes from horizon to zenith or vice versa. Each elevation angle corresponds to a specific air mass along the path. The T_{sys} from equation 2.1 can be rewritten as below,

$$T_{sys} = T_0 + T_{atm} * [1 - e^{-(\tau X_{air})}] \tag{3.2}$$

$$X_{air} = \frac{1}{\cos(90 - El)} \tag{3.3}$$

T_0 is the extrapolated noise temperature for $X_{air} = 0$ (sum of the $T_{receiver}$, T_{cover}, T_{spill}, T_{CMB})

The system temperature was measured looking at the blank sky with the antenna in continuous motion going from 90° to 30° elevation or vice versa at frequencies, 18, 22 and 25.5 GHz for the central feed. The system temperature as a function of elevation for left and right hand circular polarization of central feed is shown in Figures 3.12(18 GHz), 3.13 (22 GHz) and 3.14 (25.5 GHz). Similarly Figures 3.9, 3.10 and 3.11 show the system temperature as a function of airmass for left and right hand circular polarization of central feed. The symbols represent data and lines represent

[3]All the measurements for lateral feeds refers to the RCP only

fitting curves to the data, used to extrapolate T_0 for airmass = 0. Knowing T_0, we used equation 3.2 and measurements of T_{sys} vs elevation and airmass to calculate τ and T_{atm} from T_{sys} as listed in Table 3.2.

Table 3.2: Tipping curve measurements, τ and T_{atm} for three frequencies

Frequency (GHz)	**Polarization**	T_{atm} **(K)**	τ
18	LCP	276	0.055
18	RCP	276	0.056
22	LCP	276	0.14
22	RCP	276	0.14
25.5	LCP	276	0.088
25.5	RCP	276	0.091

The procedure used for the central feed was repeated to measure the system temperature at different elevation for the lateral feeds at 22 GHz. The opacity measured is 0.07 for this set of measurements performed in different weather conditions. Figure[4] 3.15 shows the elevation dependence of system temperature for all the feeds at 22GHz (RCP only).

[4]see note in Table 2.1

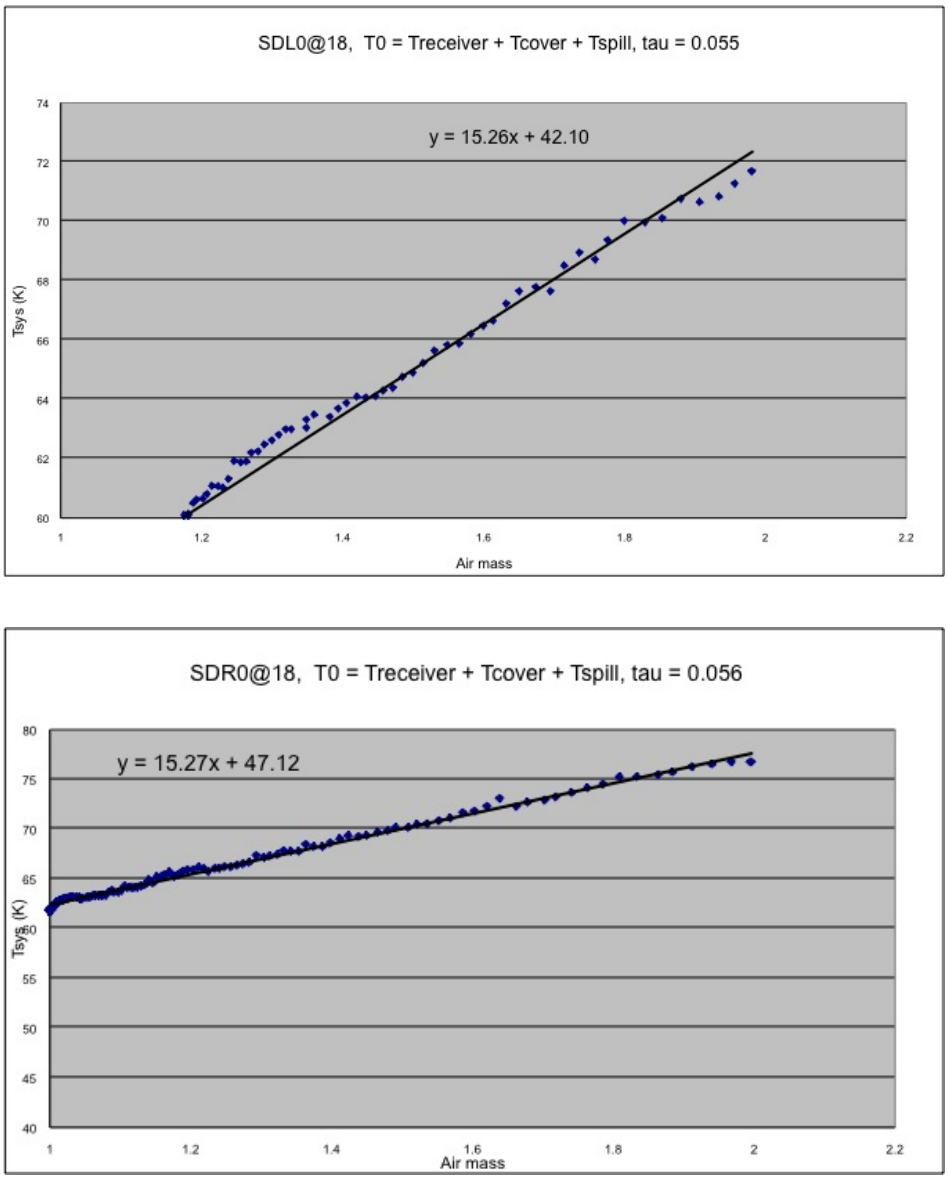

Figure 3.9: System temperature of central feed of the multi-feed receiver as a function of airmass at 18 GHz. Top: left hand circular polarization; Bottom: right hand circular polarization. Symbols represent the data; lines represent the straight line fitted to the data.

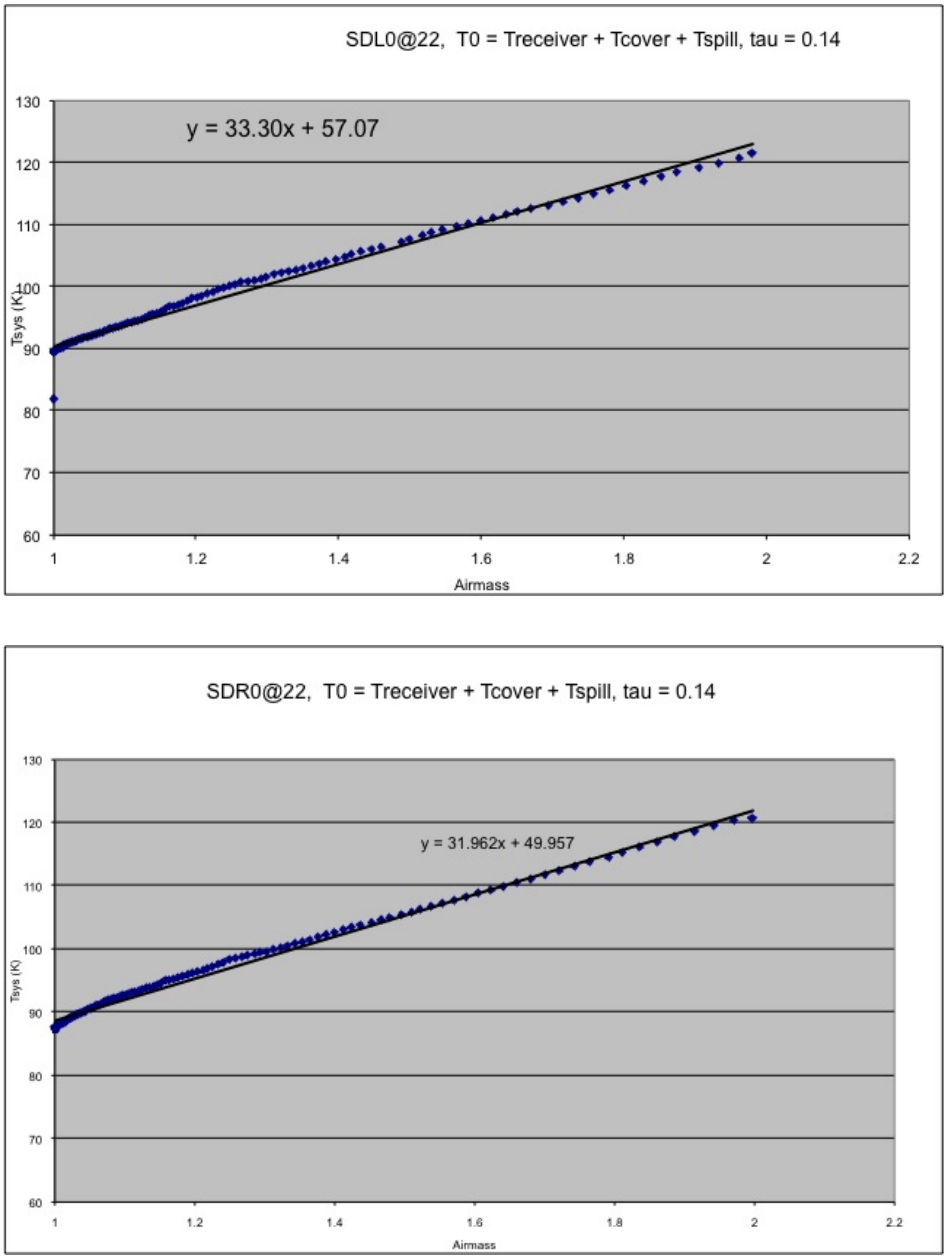

Figure 3.10: System temperature of central feed of the multi-feed receiver as a function of airmass at 22 GHz. Top: left hand circular polarization; Bottom: right hand circular polarization. Symbols represent the data; lines represent the straight line fitted to the data.

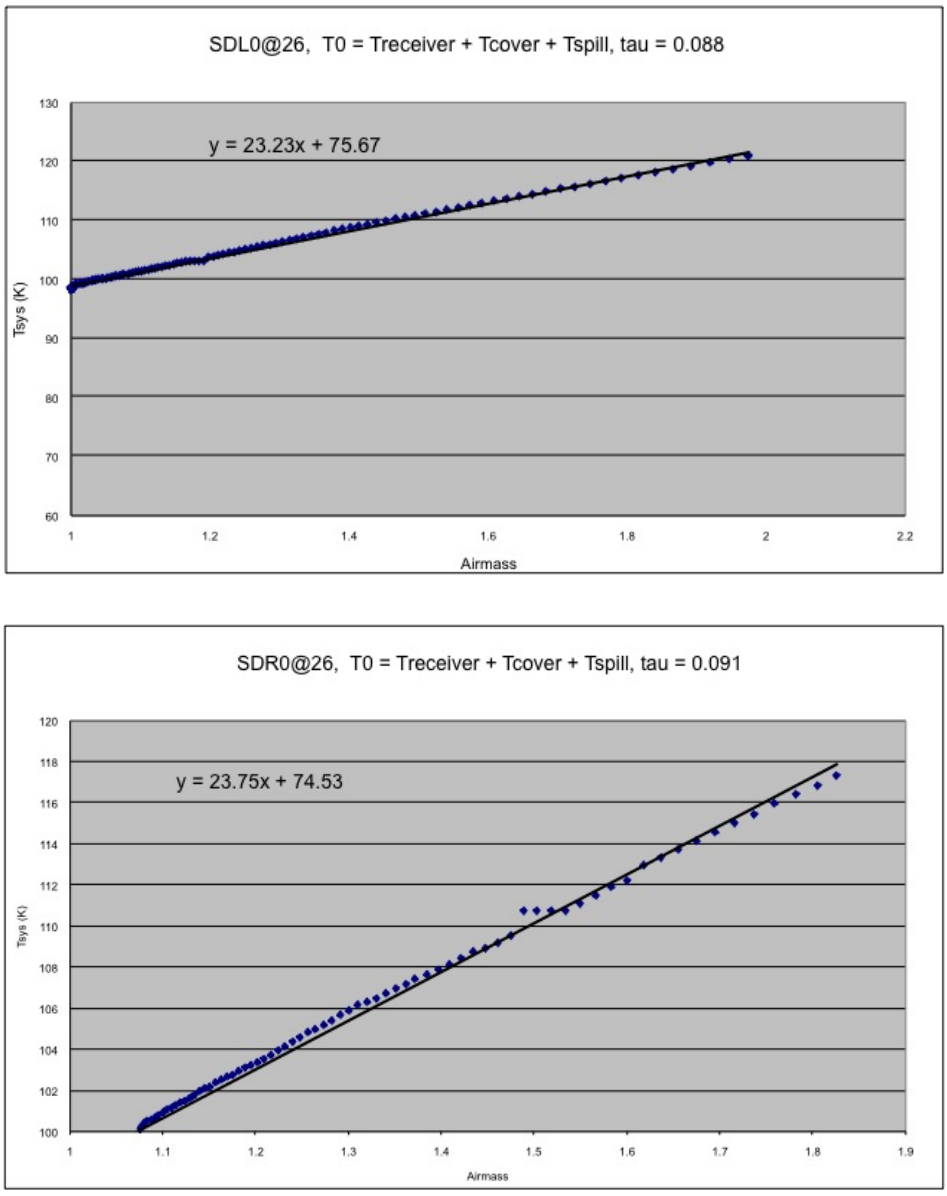

Figure 3.11: System temperature of central feed of the multi-feed receiver as a function of airmass at 25.2GHz. Top: left hand circular polarization; Bottom: right hand circular polarization. Symbols represent the data; lines represent the straight line fitted to the data.

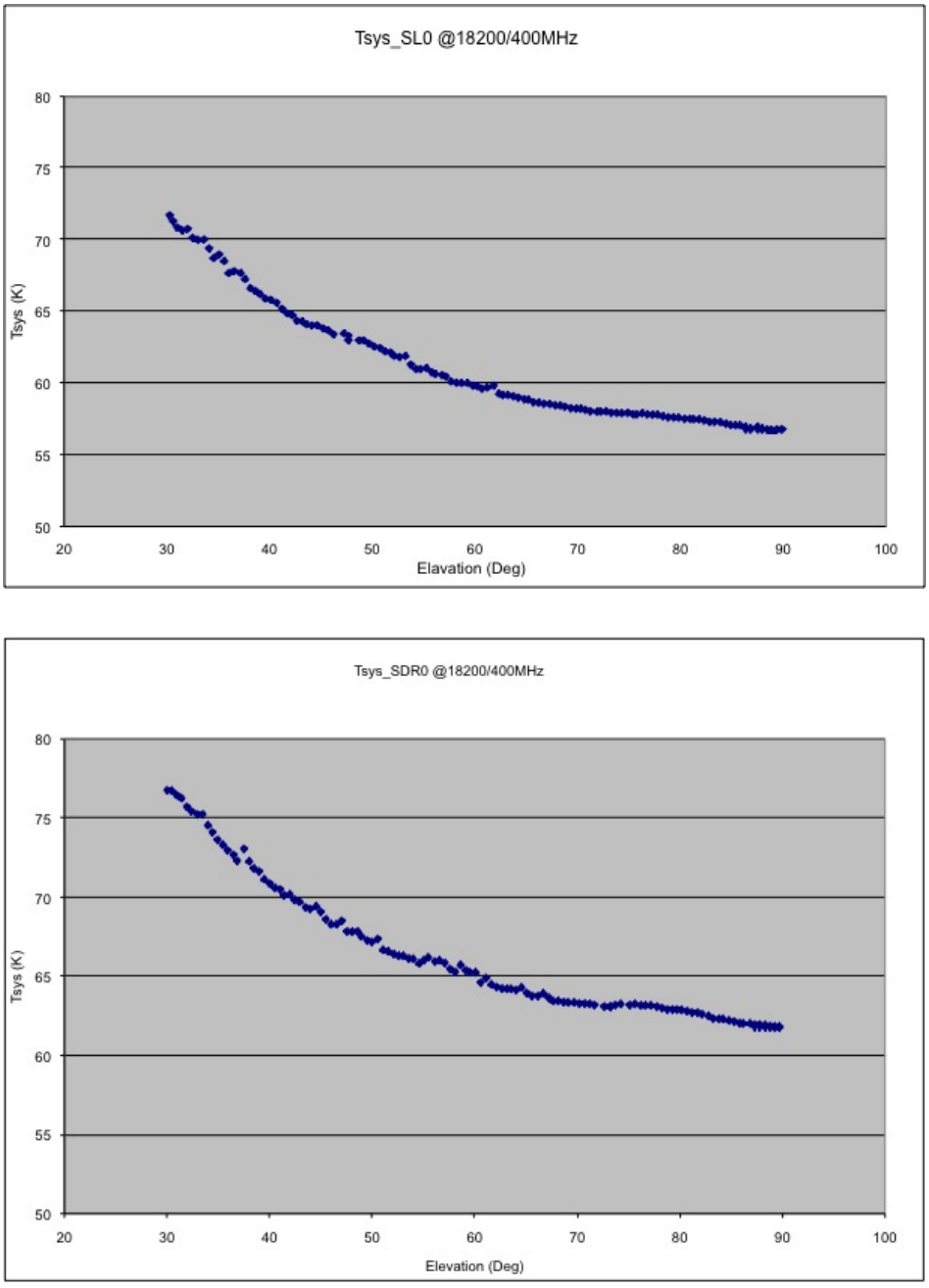

Figure 3.12: System temperature of the central horn of the multi-feed receiver as a function of elevation at 18 GHz. Top: left hand circular polarization; Bottom: right hand circular polarization.

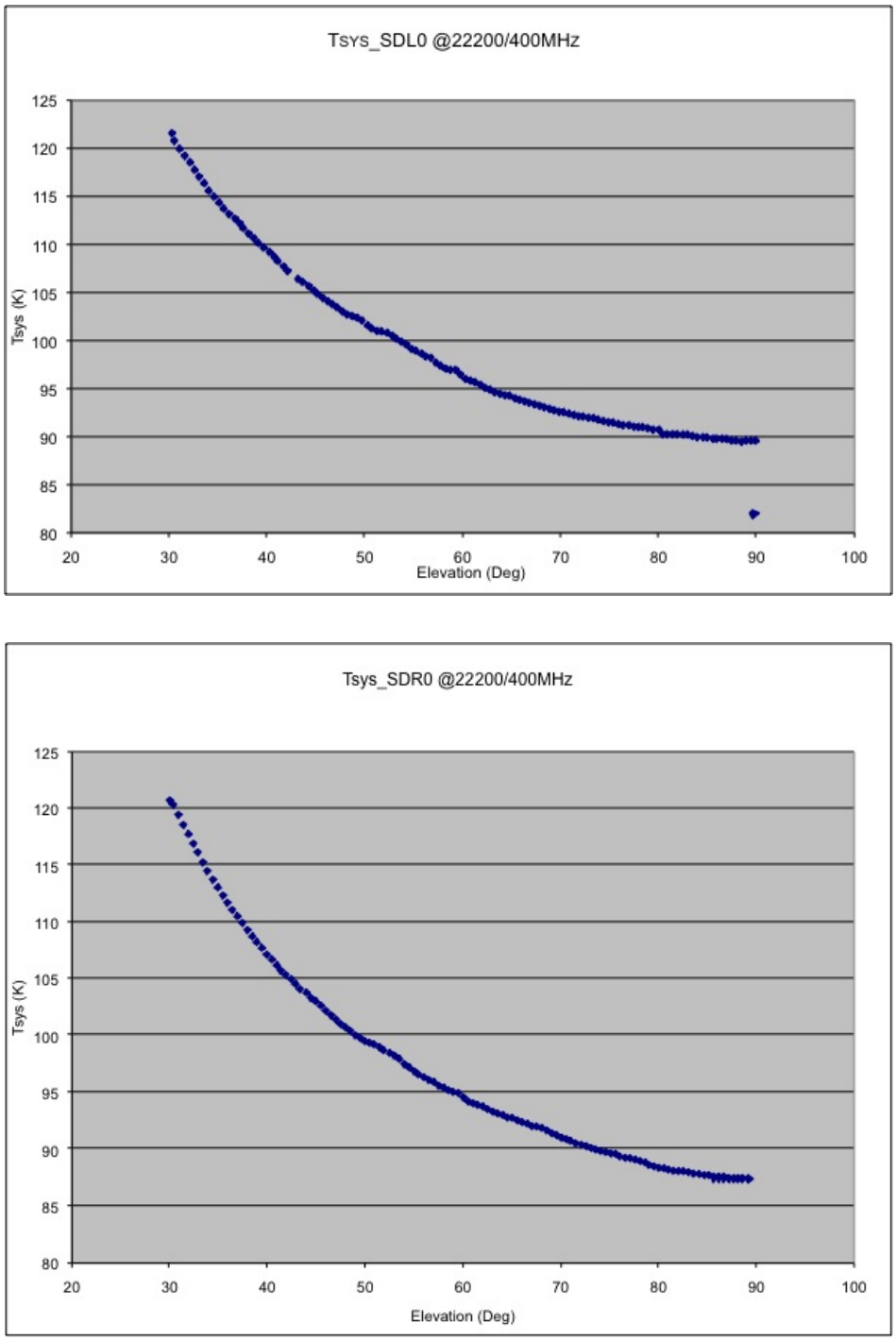

Figure 3.13: System temperature of the central horn of the multi-feed receiver as a function of elevation at 22 GHz. Top: left hand circular polarization; Bottom: right hand circular polarization.

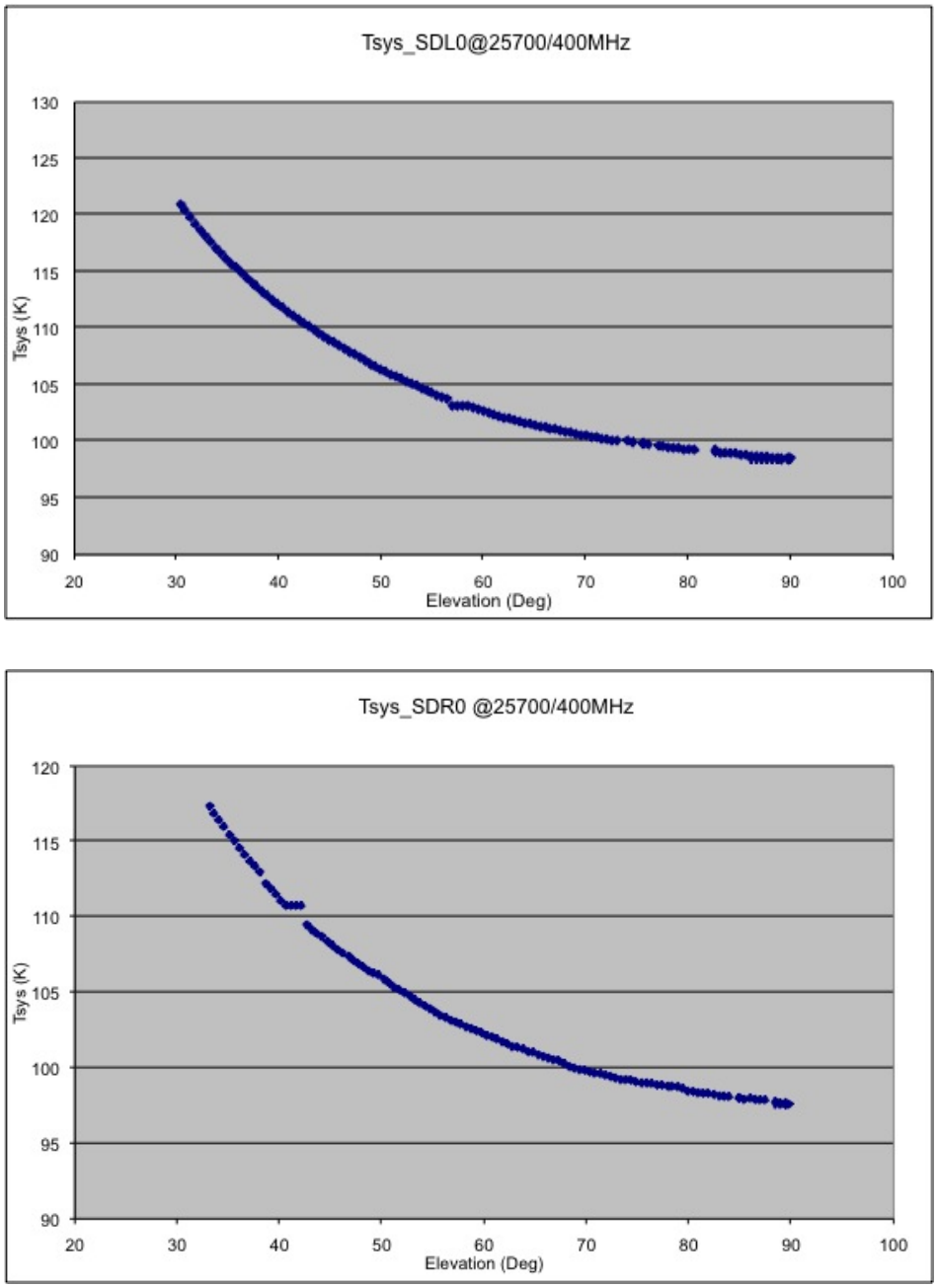

Figure 3.14: System temperature of the central horn of the multi-feed receiver as a function of elevation at 25.5 GHz. Top: left hand circular polarization; Bottom: right hand circular polarization.

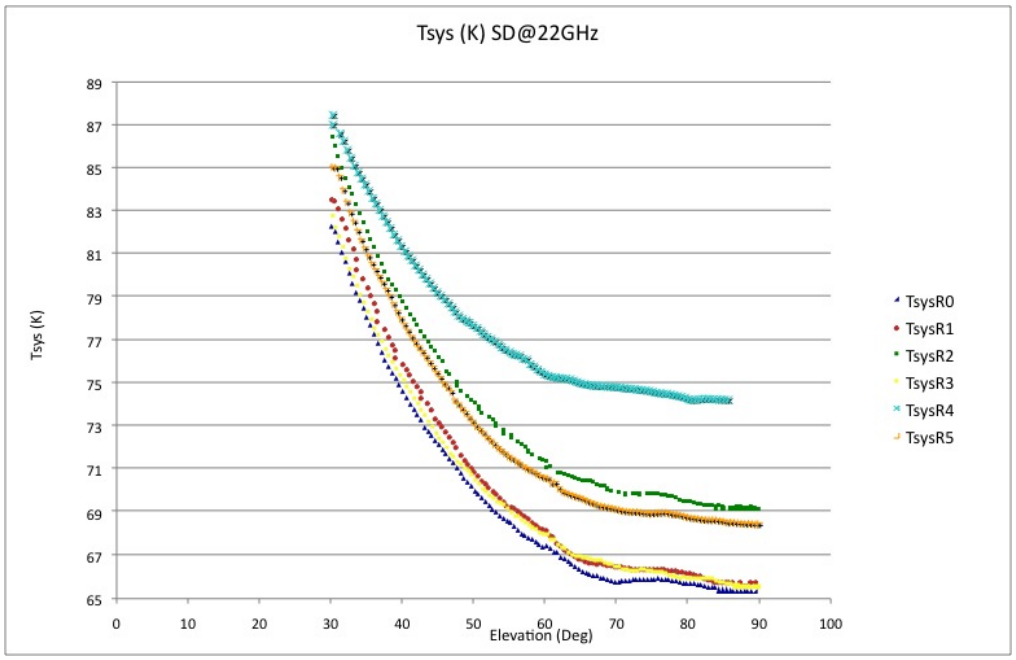

Figure 3.15: System temperature as a function of elevation for all the feeds of the 7-horn multi-feed receiver at 22 GHz (RCP only & $\tau = 0.07$)

.

3.2.2 Spillover temperature

After subtracting sky contributions corrected for the atmosphere, receiver temperature , cover and CMB from T_{sys}, we can calculate the spillover temperature. We present the spillover temperature as a function of elevation for the central feed at frequencies 18, 22 and 25.5 GHz in Figures 3.16, 3.17 and 3.18.

We calculated the spillover temperature for the lateral feeds with the same procedure used for the central feed. The spillover temperature as a function of elevation for both lateral and central feeds at frequency 22 GHz is shown in Figure[5] 3.19. The spillover temperature calculated from the system temperature measurement sets at 18 and 22 GHz is a factor of 2 higher than the estimated value.

[5] The odd feature present for horn 4 RCP is a measurement error. It does not have any physical significance.

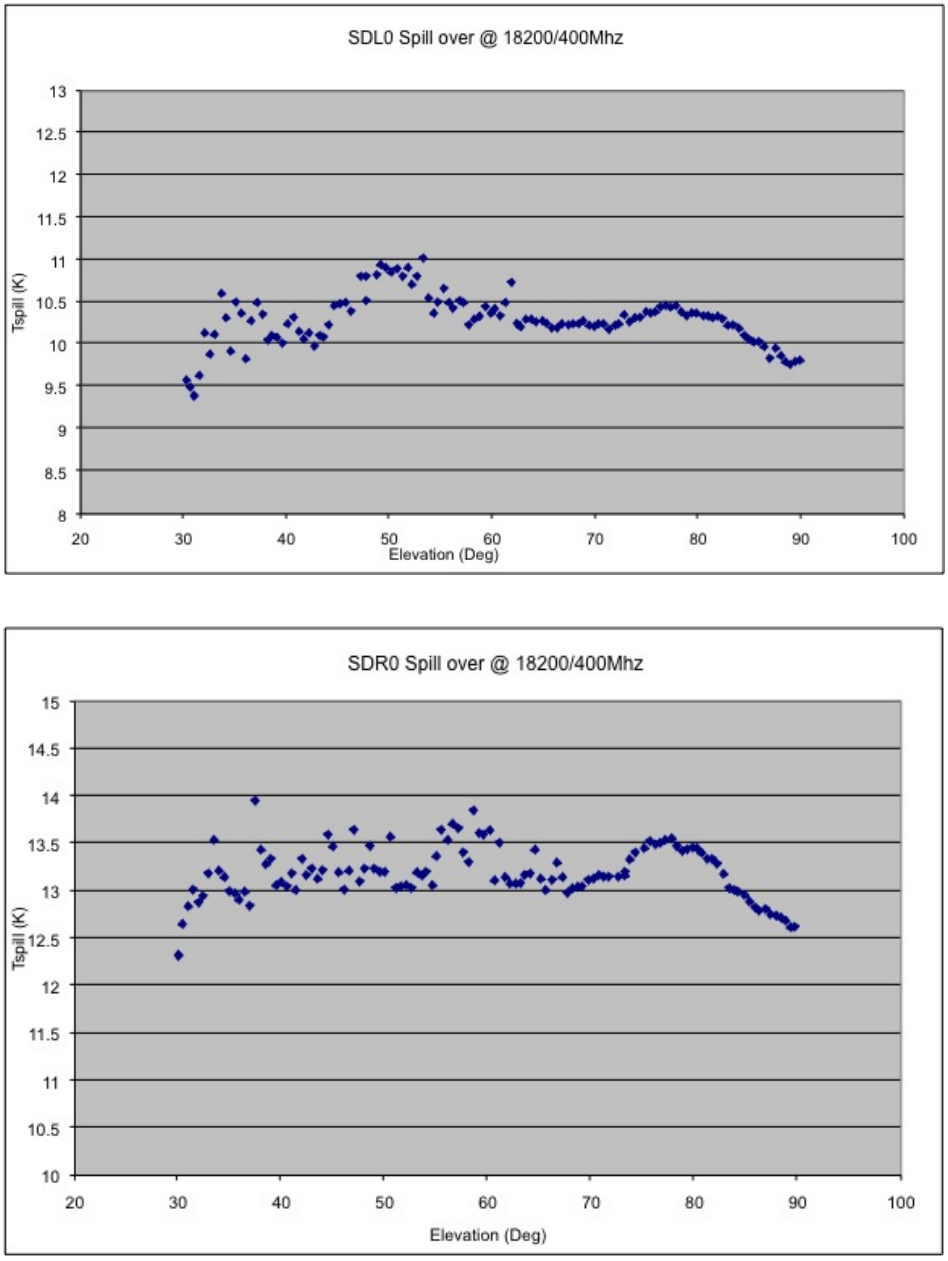

Figure 3.16: Spillover temperature of the central horn of the multi-feed receiver as a function of elevation at 18 GHz. Top: left hand circular polarization; Bottom: right hand circular polarization.

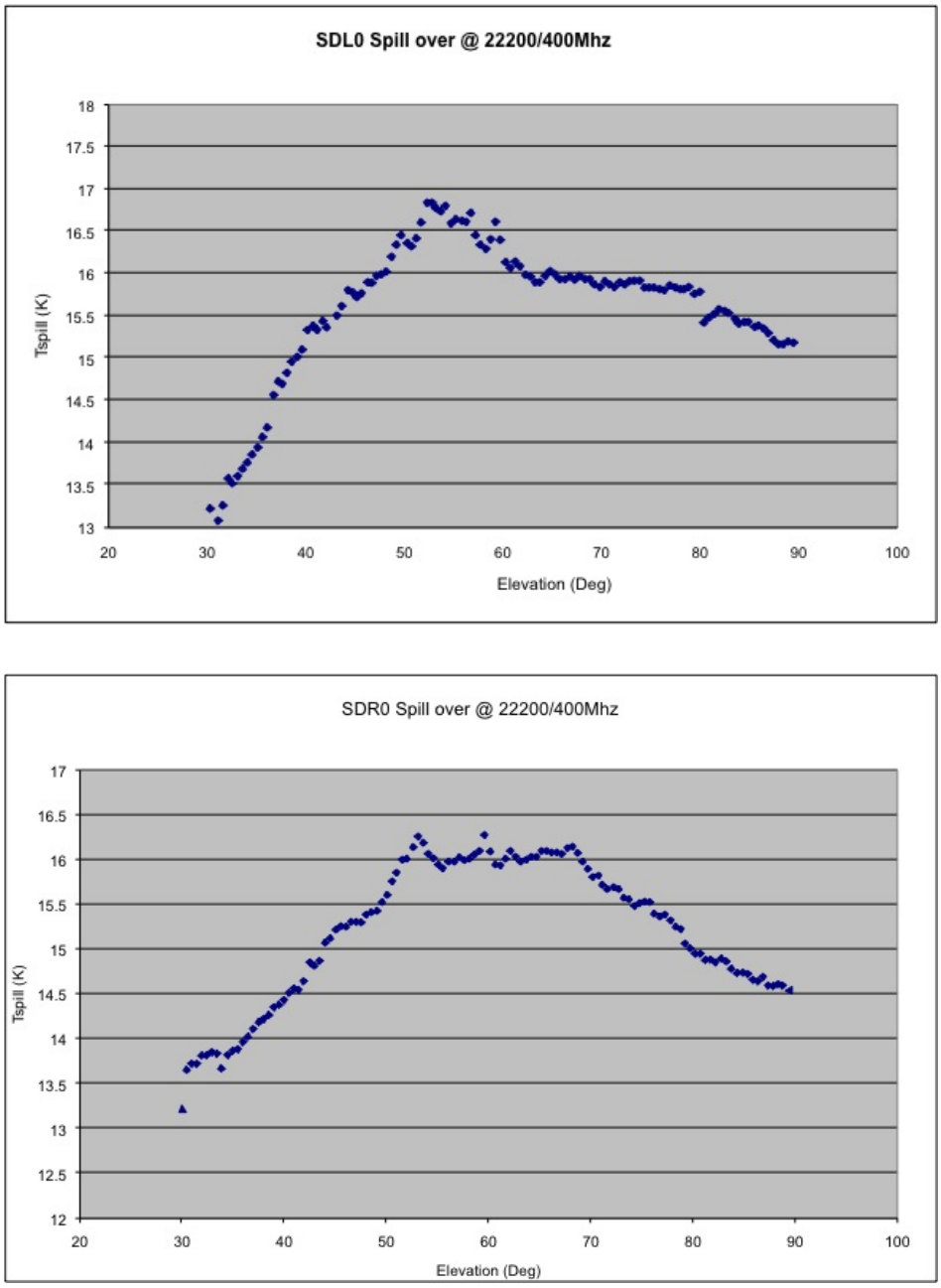

Figure 3.17: Spillover temperature of the central horn of the multi-feed receiver as a function of elevation at 22 GHz. Top: left hand circular polarization; Bottom: right hand circular polarization.

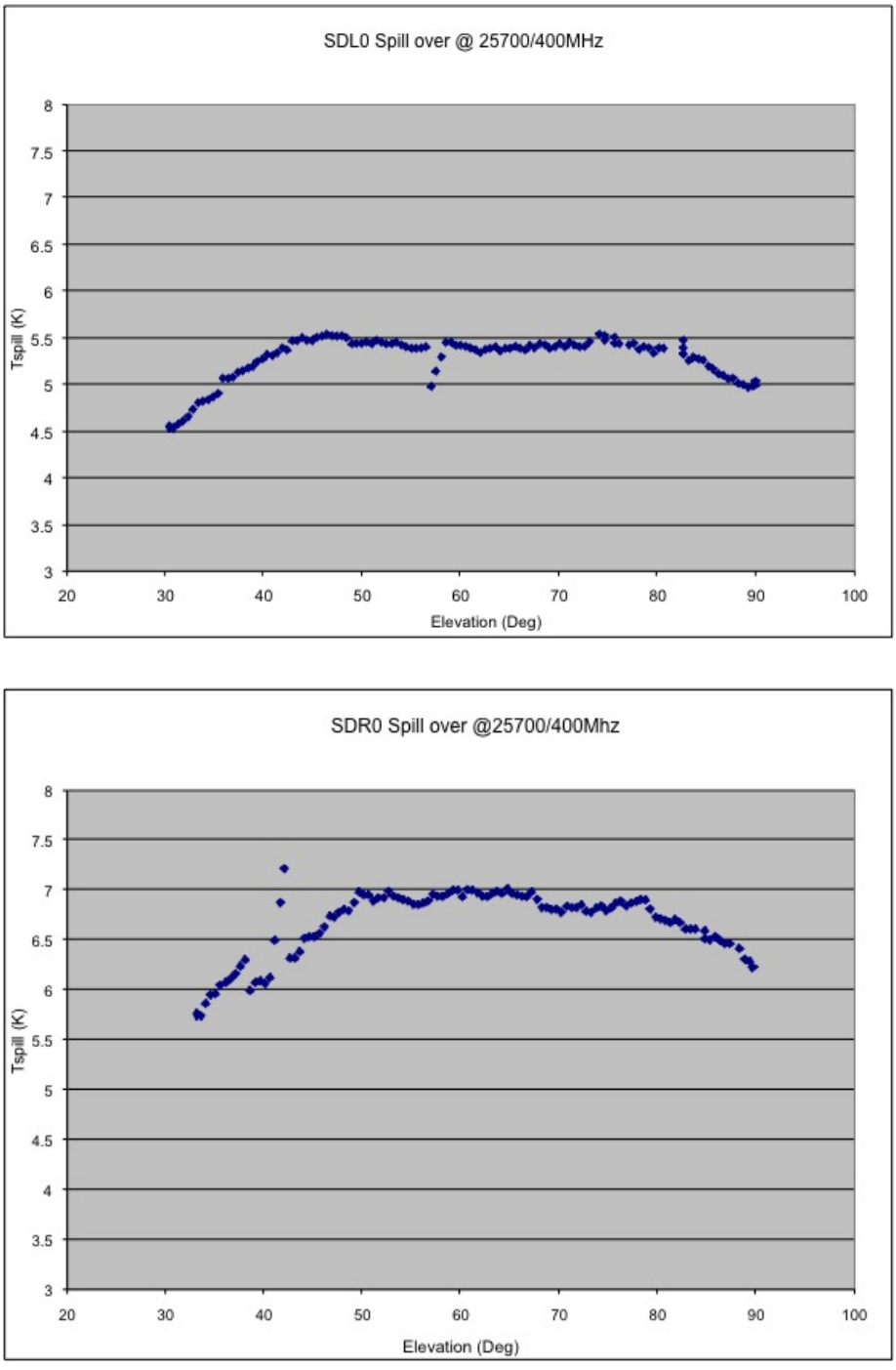

Figure 3.18: Spillover temperature of the central horn of the multi-feed receiver as a function of elevation at 25.5 GHz. Top: left hand circular polarization; Bottom: right hand circular polarization.

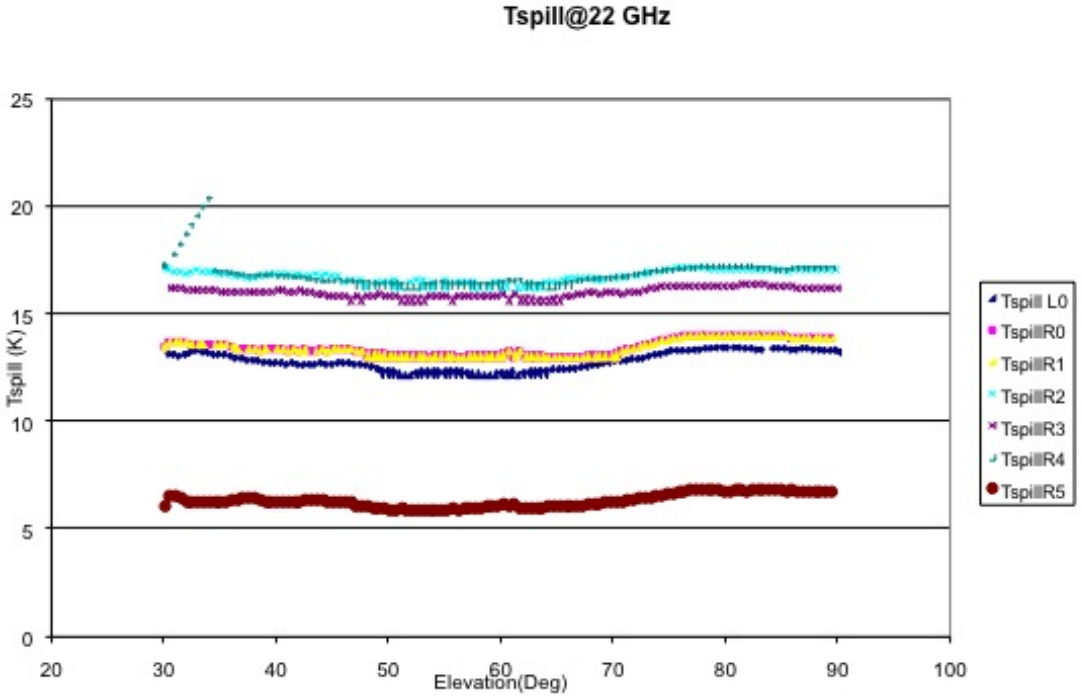

Figure 3.19: Spillover temperature for the lateral feeds and central feed of multi-feed receiver at 22GHz

3.2.3 Antenna gain

An evenly illuminated telescope has a gain curve that varies with telescope's zenith angle (elevation) in a predictable manner. It is always recommended to provide the telescope gain curve to the observer a priori. The telescope gain curve at different elevations is obtained by observing radio sources of known flux density. In order to retrieve the telescope gain curve we observed source DR21 with the multi-feed receiver. Source DR21 is a bright source used as a primary calibrator at high frequency.

3.2.3.1 Central feed gain

Figure 3.20 shows the elevation dependence of the antenna gain as measured by observing source DR21 with the central horn of the multi-feed receiver. The antenna gain as measured on source DR21 is less than the estimated value (see Table 2.4). We are explaining possible reasons. One possible explanation for this discrepancy is a measurement error of the sky contribution (T_{atm}, τ).

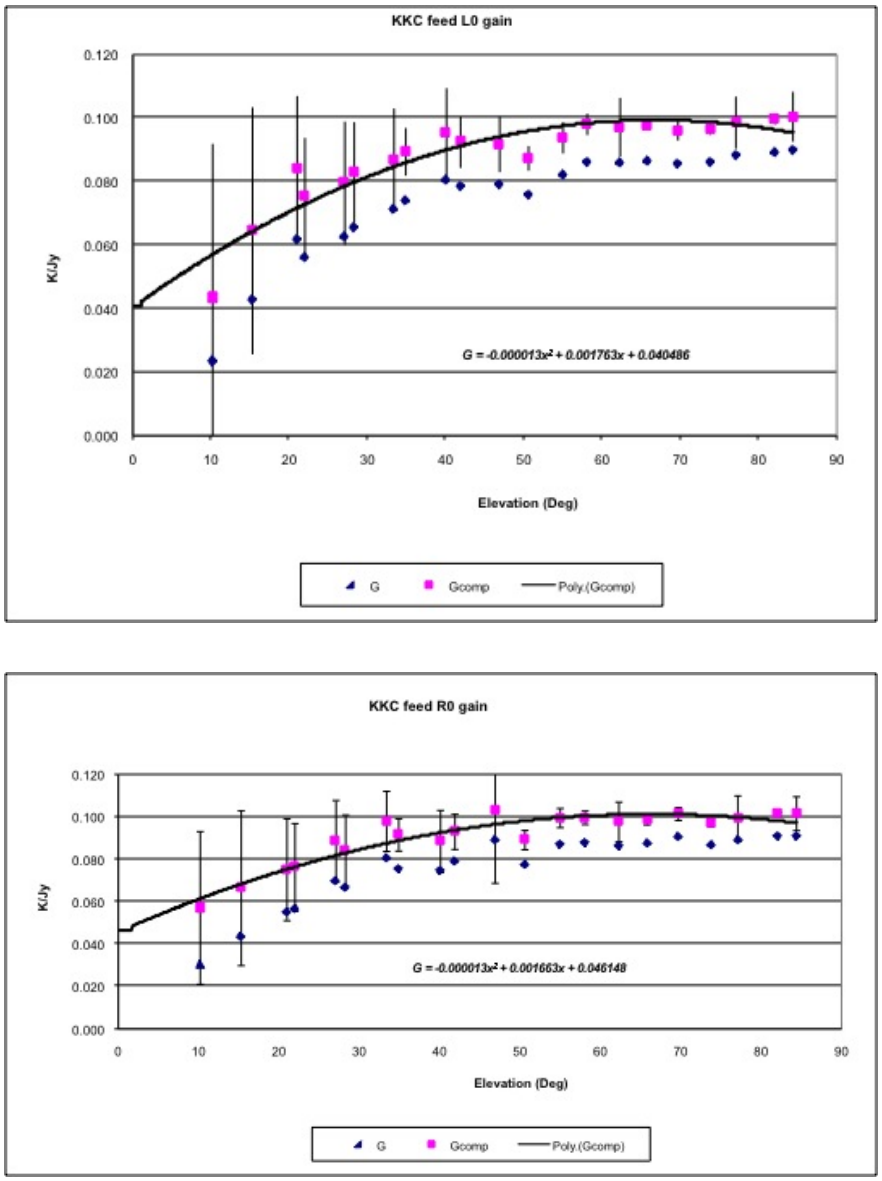

Figure 3.20: Antenna gain of the central horn of the multi-feed receiver, as measured by observing source DR21 at different elevations. Blue diamonds represent the data, pink squares show the data corrected for opacity and the line represents the polynomial curve fitted to the data corrected for opacity. Top: left hand circular polarization; Bottom: right hand circular polarization.

3.2.3.2 Lateral feed gain

The same procedure was repeated to measure the gain of lateral feeds. The antenna gains of lateral feeds relative to central one are presented in Tables 3.3, 3.4 and 3.5, together with other relevant parameters. The antenna gain of lateral feeds are presented separately because they have been obtained in three different measurement sets, performed in different weather conditions. The average value for the antenna gain for the lateral feeds is approximately 98% of the central feed gain.

Table 3.3: Antenna gain of feeds 1 and 4 relative to central feed 0 (RCP)

Feed Number	T_{sys} K	$T_{receiver}$ K	T_{diff}[a] **K**	T_{diff} **ratio**[b]	T_a **K**	**Gain**[c]
0	75.0	26.0	49.0	1.00	1.50	1.00
1	75.5	22.0	53.5	1.09	1.46	0.97
4	85	30.8	54.2	1.11	1.43	0.95

[a] $T_{sys} - T_{receiver}$
[b] T_{diff}(lateral feed) / T_{diff}(central feed)
[c] Gain relative to central feed

Table 3.4: Antenna gain of feeds 2 and 5 relative to central feed 0 (RCP)

Feed Number	T_{sys} K	$T_{receiver}$ K	T_{diff} **K**	T_{diff} **ratio**	T_a **K**	**Gain**
0	77.0	26.0	51.0	1.00	1.50	1.00
2	80.5	25.8	54.7	1.07	1.48	0.99
5	80.0	35.4	44.6	0.87	1.45	0.97

Table 3.5: Antenna gain of feed 3 relative to central feed 0 (RCP)

Feed Number	T_{sys} K	$T_{receiver}$ K	T_{diff} **K**	T_{diff} **ratio**	T_a **K**	**Gain**
0	75.0	26.0	49.0	1.00	1.55	1.00
3	74.0	23.0	51.0	1.04	1.5	0.97
6[a]	na	na	na	na	na	na

[a]see note in Table 2.1

3.2.4 Sky distance between adjacent feeds & horn Half Power Beam Width

To measure the sky separation between adjacent feeds and the HPBW of each feed we performed cross scans of source DR21 at 22 GHz. We aligned the axis of feeds 1, 0 and 4, with the azimuth axis of the antenna (Figure 3.21) using the derotator, mounted on the Medicina dish, and performed an elevation scan of the source with each feed to check the feed azimuth alignment.

Figure 3.22 shows the elevation scan of source DR21. Green and yellow lines represent the scan of feed 1[6](RCP) and red and blue lines correspond to the scans of feed number 0 and 4 respectively (RCP). As Figure 3.22 shows, all three feeds are pointing at the same elevation in the sky indicating that the 1-0-4 axis is well aligned with the azimuth axis of the antenna. Similarly we performed an azimuth scan of source DR21.

Figure 3.23 shows the azimuth scan of source DR21 for feeds 1,0 and 4 respectively (RCP). Green, red and blue lines represent feed number 1, 0 and 4 respectively, and black line shows the Gaussian fitting to the data to measure the HPBW.
The same procedure was followed for feeds 2, 0, 5 and 3 ,0, 6 in order to measure the HPBW and the sky distance between adjacent horns for these groups of feeds as well.
Table 3.6 summarizes HPBW fitted values and sky distance between adjacent feeds in both azimuth and elevation axes.

[6]The scan sequence is 1- 0 - 4 - 0 therefore for feed 0 (central) we have two scans: one in forward and one in backward direction

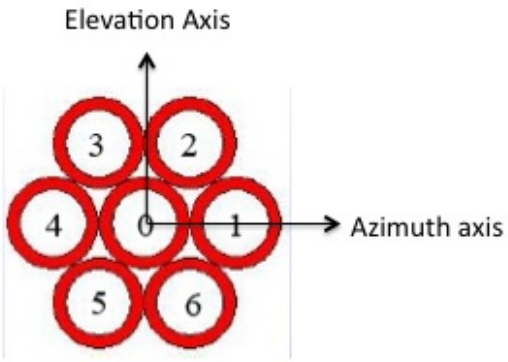

Figure 3.21: Geometry of the multi-feed receiver after aligning the 4-0-1 feed-axis to the azimuth axis of the antenna

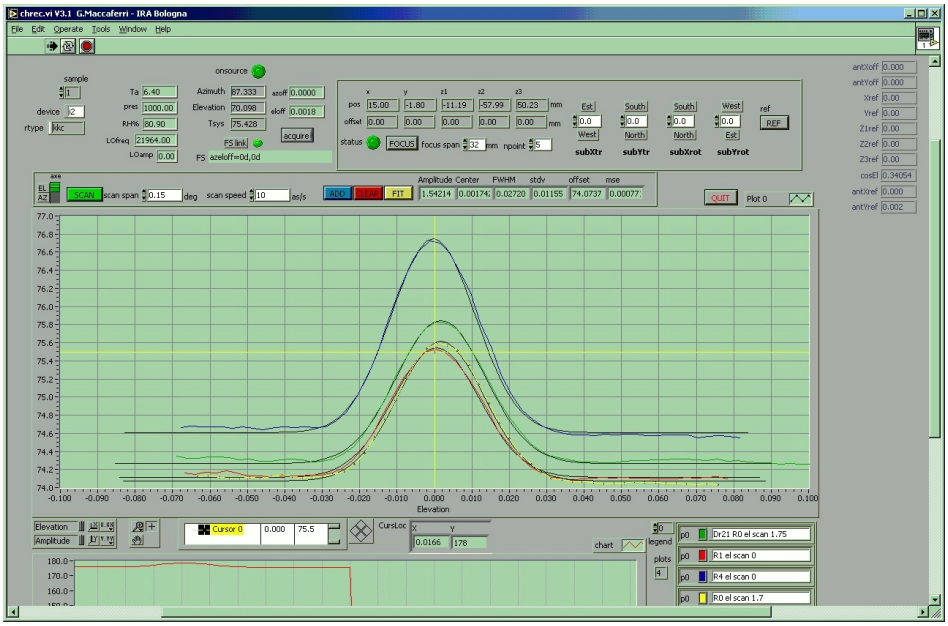

Figure 3.22: Elevation scans of source DR21 performed with feeds 1,0 and 4. Green and yellow lines represent feed number 1 while red and blue lines represent feeds 0 and 4 respectively (RCP).

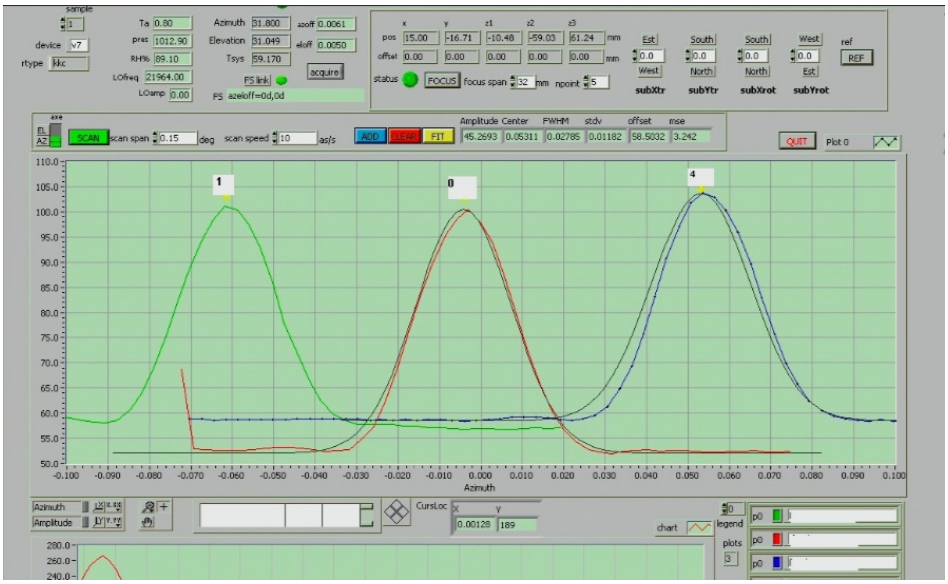

Figure 3.23: The green, red and blue lines represent the azimuth scans of source DR21 at an elevation of 31° performed with feed number 1, 0 and 4 respectively (RCP)

Table 3.6: HPBW and sky distance between adjacent feeds with reference to the central feed

Feed Number	X_{disp} [a] deg	Y_{disp} [b] deg	X_{disp} arcsec	Y_{disp} arcsec	$HPBW$ arcsec
0	0.00	0.00	0.00	0.00	90.0
1	0.058	0.002	209.0	7.00	93.6
2	0.030	- 0.051	108.0	- 184.0	97.2
3	- 0.030	- 0.050	- 108.0	-180.0	93.6
4	- 0.060	0.002	- 216.0	7.00	93.6
5	- 0.029	0.053	- 104.0	191.0	97.2
6[c]	na	na	na	na	na

[a]Azimuth offset relative to central horn (sky distance between adjacent feeds on azimuth axis)

[b]Elevation offset relative to central horn (sky distance between adjacent feeds on elevation axis)

[c]see note in Table 2.1

3.3 Summary and Future Work

A pointing calibration campaign was carried out for the central feed of the K-band multi-feed receiver mounted on the Medicina 32 m dish. We optimized the optical alignment of the telescope. We implemented the new subreflector model for the optimized alignment and the new antenna-pointing model for the multi-feed receiver in the antenna control system. We measured antenna characteristic parameters, like system, spillover and antenna temperatures, HPBW of each feed and sky distance between adjacent feeds for the 7-horn multi-feed receiver. Most of the parameters are in agreement within the measurement errors with the laboratory measurements. However we have noticed that the antenna gain for the K-band multi-feed receiver is less than estimated from simulations. Also the spillover temperature from the test measurements is a factor of 2 higher than the estimated value. The reason for these discrepancies could be explained with an error in the sky contribution measurements. We are now developing new, more sophisticated procedures to estimate τ and T_{atm} in order to check this hypothesis.

Acknowledgements

R.Verma would like to thank Franco Mantovani for the arduous task of proof reading.
This research was supported by the EU Framework 6 Marie Curie Early Stage Training programme under contract number MEST-CT-2005-19669 '*ESTRELA*'.

Bibliography

[1] **J.D. Kraus**, *'Radio Astronomy', McGraw Hill, 1966*

[2] **Constantine A. Balanis**, *'ANTENNA THEORY: ANALYSIS AND DESIGN', 3rd edition; Wiley Interscience*

[3] **Edited by : Darrel T. Emerson and John M. Payne**, *'MULTI-FEED SYSTEMS FOR RADIO TELESCOPE', Astronomical Society of the Pacific Conference Series, Volume 75*

[4] **E. Cenacchi, A.Orfei**, *SRT: multi-feed RECEIVERS, Internal Report, IRA 384/06*

[5] **A.Orfei, M. Morsiani, G. Zacchiroli, G. Maccaferri**, *'Il nuovo sistema di posizionamento del subriflettore e dei ricevitori in fuoco primario per l'antenna VLBI di Medicina', Internal Report, IRA 260/98*

[6] **A.Orfei**, *'PARABOLIC ANTENNAS', WILEY ENCYCLOPEDIA OF TELECOMMUNICATIONS - Parabolic Antennas, 2003*

[7] **K.O'Neil**, *'Single Dish Calibration Technique at Radio Wavelengths', 2002,ASP Conference Series, 278, 293O*

[8] **Donald B. Compbell**, *'Measurements in Radio Astronomy', 2002, ASP Conference Series, 278, 81C*

[9] **Paul F. Goldsmith**, *'Radio Telescope and Measurements at Radio Wavelengths', 2002, ASP Conference Series, 278, 45G*

[10] **P. R. Jewell**, *'Millimeter Wave Calibration Technique', 2002, ASP Conference Series, 278, 313J*